Knowl. Manag. Aquat. Ecosyst. 2025, 426, 11
© K. Ilgen *et al.*, Published by EDP Sciences 2025
https://doi.org/10.1051/kmae/2025008

www.kmae-journal.org

Knowledge & Management of Aquatic Ecosystems

Journal fully supported by Office français de la biodiversité

RESEARCH PAPER OPEN ACCESS

Hydrological and ecological effects of floating photovoltaic systems: a model comparison considering mussel, periphyton, and macrophyte growth

Konstantin Ilgen[1,2,*], Camila Bergmann Goulart[3,4], Stephan Hilgert[5], Dirk Schindler[6], Klaus van de Weyer[7], Rafael de Carvalho Bueno[8], Tobias Bleninger[3], Raffaello Lastrico[1,2], Leonhard Gfüllner[1], Alexander Graef[1], Stephan Fuchs[4] and Jens Lange[2]

[1] Fraunhofer Institute for Solar Energy Systems ISE, Freiburg, Baden-Württemberg, Germany
[2] Hydrology, Faculty of Environment and Natural Resources, University of Freiburg, Freiburg, Baden-Württemberg, Germany
[3] Post-Graduate Programme on Water Resources and Environmental Engineering, Federal University of Paraná, Curitiba, Paraná, Brazil
[4] Water Quality Management, Institute for Water and Environment, Karlsruhe Institute of Technology, Karlsruhe, Baden-Württemberg, Germany
[5] limknow GmbH & Co. KG, Karlsruhe, Germany
[6] Environmental Meteorology, Faculty of Environment and Natural Resources, University of Freiburg, Freiburg, Baden-Württemberg, Germany
[7] Lanaplan GbR, Nettetal, Germany
[8] Post-Graduate Programme on Environmental Engineering, Federal University of Paraná, Curitiba, Paraná, Brazil

Received: 14 October 2024 / Accepted: 10 April 2025

Abstract – Floating photovoltaic (FPV) systems are increasingly deployed on gravel pit lakes to generate renewable energy and mitigate land-use conflicts. However, their environmental impacts on hydrological and ecological processes remain insufficiently studied. This study investigates the effects of a 1.5-MWp FPV system covering 8% of a 19-ha gravel pit lake in Germany. The General Lake Model (GLM-AED2) and Delft3D-FLOW were used to simulate FPV-induced changes. Meteorological data—including irradiance, air temperature, wind speed, and relative humidity—were recorded above and below the PV modules. Water quality data—including water temperature, dissolved oxygen, pH, dissolved organic carbon, and chlorophyll-*a*—were collected beneath the FPV and in open water. Mussel colonisation of the FPV substructure was assessed, and its filtration impact on water quality analysed. Macrophyte distribution was assessed beneath the FPV system and along the shorelines. Results showed a modelled 88% solar irradiance and 57% wind speed reduction beneath the FPV system. Water quality impacts were minimal and primarily influenced by mussels colonising the substructure. Macrophytes occurred in littoral zones up to 5.25 m deep up to 5.25 m deep, but habitat-typical species were scarce due to gravel extraction and herbivorous fish. These findings highlight complex interactions between FPV, mussel filtration, macrophytes, and human activities, suggesting that other anthropogenic factors may outweigh FPV impacts. Model simulations indicated that FPV coverage above 45% could destabilise thermal stratification and alter primary production. This study underscores the need for empirical monitoring and modelling to optimise FPV deployment and inform regulatory frameworks for sustainable development.

Keywords: Floating solar / environmental impact / hydrodynamic modelling / quagga mussel / macrophyte abundance

1 Introduction

Floating photovoltaic (FPV) is an innovative technology that generates renewable electricity and reduces greenhouse gas emissions. Unlike ground-mounted and rooftop photovoltaic (PV) systems, FPV extends solar deployment across inland and offshore waters, reducing land-use conflicts. As such, FPV offers an additional opportunity to address global challenges such as climate change, increasing energy demand, and land scarcity (World Bank Group *et al.*, 2019a; Xia *et al.*, 2023; Nobre *et al.*, 2024). Furthermore, synergies can be expected from coupling with other forms of energy generation, such as hydropower or wind (Lee *et al.*, 2020; Kakoulaki *et al.*, 2023; Ogunjo *et al.*, 2023). The expansion of FPV has been dynamic

*Corresponding author: konstantin.ilgen@ise.fraunhofer.de

This is an Open Access article distributed under the terms of the Creative Commons Attribution License CC-BY-ND (https://creativecommons.org/licenses/by-nd/4.0/), which permits unrestricted use, distribution, and reproduction in any medium, provided the original work is properly cited. If you remix, transform, or build upon the material, you may not distribute the modified material.

in recent years, with significant growth in Asia and Europe, where many projects are either operational or in the planning stage (World Bank Group *et al.*, 2019b). Although most FPV installations in Europe are constructed on artificial waterbodies such as gravel pit lakes and reservoirs, their environmental impacts remain insufficiently studied (Nobre *et al.*, 2024). In Germany, current legislation limits FPV coverage to 15% of the water surface and mandates a minimum distance of 40m from the shore (Bundesamt für Justiz, 2023). However, these limits do not have an empirical basis, underscoring the need for further research on ecological consequences. A comprehensive review of FPV's potential environmental impacts on aquatic ecosystems identified key influencing factors such as system design, site-specific conditions, and meta-ecosystem dynamics (Nobre *et al.*, 2023).

Previous studies have investigated FPV impacts on lake processes using various hydrodynamic models. Ji *et al.* (2022) employed the CE-QUAL-W2 model to simulate FPV effects on the Xiangjiaba Reservoir in China. They reported water temperature reductions and changes in thermal stratification, with effects extending beyond the FPV-covered area, influencing approximately 20% of the reservoir's total length. A maximum reduction in surface water temperature below FPV of up to 3.3 °C was simulated, and the reservoir was predicted to benefit from reduced evaporation of up to 35 million m^3. Exley *et al.* (2021) studied the effects of an FPV system on Windermere, England, using the MyLake model and suggested that a larger FPV coverage was positively correlated with a stronger reduction in water temperature. Their study found that FPV reduced water temperature by up to 8.0 °C and significantly affected stratification stability. Similarly, Ilgen *et al.* (2023) observed a 2.8 °C cooling effect in a German gravel pit lake with a 750 kWp FPV system due to a 73% reduction in solar irradiance. On-site measurements were used to calibrate the General Lake Model (GLM), with simulations indicating that FPV coverages below 15% had minimal influence on stratification, whereas notable changes occurred above 50%. These studies revealed two opposing FPV effects on lake stratification: reduced irradiance lowers energy input and weakens stratification, whereas reduced wind shear limits vertical mixing and stabilises stratification. This interplay highlights the complexity of physical processes in FPV-covered lakes. Empirical validation of these mechanisms is essential to enhance hydrodynamic model accuracy. Moreover, previous research suggests that FPV may mitigate certain climate change effects on lake ecosystems.

Other modelling studies examined FPV influences on chemical and biological lake processes. Yang *et al.* (2022) coupled the Estuary, Lake, and Coastal Ocean Model (ELCOM) with the Computational Aquatic Ecosystem Dynamics Model (CAEDYM) to simulate FPV impacts on a shallow tropical reservoir in Singapore. Their results indicated increased thermal stability at 30% FPV coverage, alongside reductions in chlorophyll-*a*, total organic carbon, and dissolved oxygen by 30%, 15%, and 50%, respectively, while total nitrogen and phosphorus concentrations increased. Haas *et al.* (2020) applied the ELCOM-CAEDYM model to a hydropower reservoir in Chile, finding that FPV occupancies between 40% and 60% could help to prevent algal blooms while maintaining hydropower efficiency. Exley *et al.* (2022) used the MyLake model to assess phytoplankton dynamics in a reservoir in England, demonstrating that a 10% FPV coverage reduced chlorophyll-*a* concentrations by 17% to 48%, depending on seasonal variability. Karpouzoglou *et al.* (2020) simulated FPV impacts on primary production in a brackish water system in the Netherlands using the General Ocean Turbulence Model (GOTM) coupled with the European Regional Seas Ecosystem Model (ERSEM-BFM). They found that FPV occupancies below 20% had negligible effects, but above this threshold, net primary production declined significantly. Château *et al.* (2019) used the Simulation Modelling System for Aquatic Bodies (SIMSAB) to predict FPV effects on fishponds in Taiwan. While FPV slightly reduced fish production due to lower dissolved oxygen, it provided substantial energy gains, suggesting an overall benefit of FPV integration into aquaculture systems.

The introduction of FPV structures into water bodies creates new colonisation opportunities for sessile organisms, including native species and invasive mussels such as the quagga *(Dreissena rostriformis bugensis)* and zebra mussels (*Dreissena polymorpha*). The quagga mussel, originally from Eastern Europe, was first observed in Western Europe in 2006 and has since s rapidly spread through major rivers such as the Rhine and Danube at an average rate of 120 km per year (Orlova *et al.*, 2004; Son, 2007; Matthews *et al.*, 2014). By filtering water, mussels remove plankton, nutrients, and suspended matter, potentially altering aquatic ecosystems (Rowe *et al.*, 2017). Their colonisation of technical infrastructure can cause economic damage to waterworks and fisheries (Connelly *et al.*, 2007). Quagga mussels form a mutually beneficial relationship with Nuttall's waterweed (*Elodea nuttallii*), as filtration improves light penetration, enhancing plant growth, while dense macrophyte stands provide habitat for mussels (Wegner *et al.*, 2019). This accelerates their spread and intensifies competition with native species, posing a significant threat to freshwater ecosystems. Under a colonised FPV system, two opposing processes occur: the reduction of solar irradiance, due to shading, is confined to the FPV area, while filtering mussels increase water clarity beneath the installation which may extend across the entire lake, including shoreline habitats, and thus influence the depth of the euphotic zone. As both mussel filtration and FPV-induced changes in light availability affect underwater vegetation dynamics, their combined impact on macrophyte growth and competition remains largely unexplored. While modelling may provide valuable insights into FPV effects, empirical validation is essential to improve predictive accuracy. Field data are required to refine model outputs and assess broader ecological implications, including shifts in trophic interactions.

This study aims to (1) empirically assess the dominant factors influencing water quality in FPV lakes by comparing FPV-induced changes with external drivers such as inflows and excavation activities, (2) evaluate the capability of two hydrodynamic models (Delft3D-FLOW and GLM–AED2) to simulate FPV-induced changes by validating model outputs with *in situ* data and predicting long-term effects under higher FPV coverage scenarios (15%, 30%, 45%, and 90%), (3) investigate the relationship between empirically estimated mussel filtration due to colonisation on FPV structures and modelled macrophyte growth responses resulting from increased water clarity, and (4) assess the suitability of current FPV regulations by integrating empirical field data and

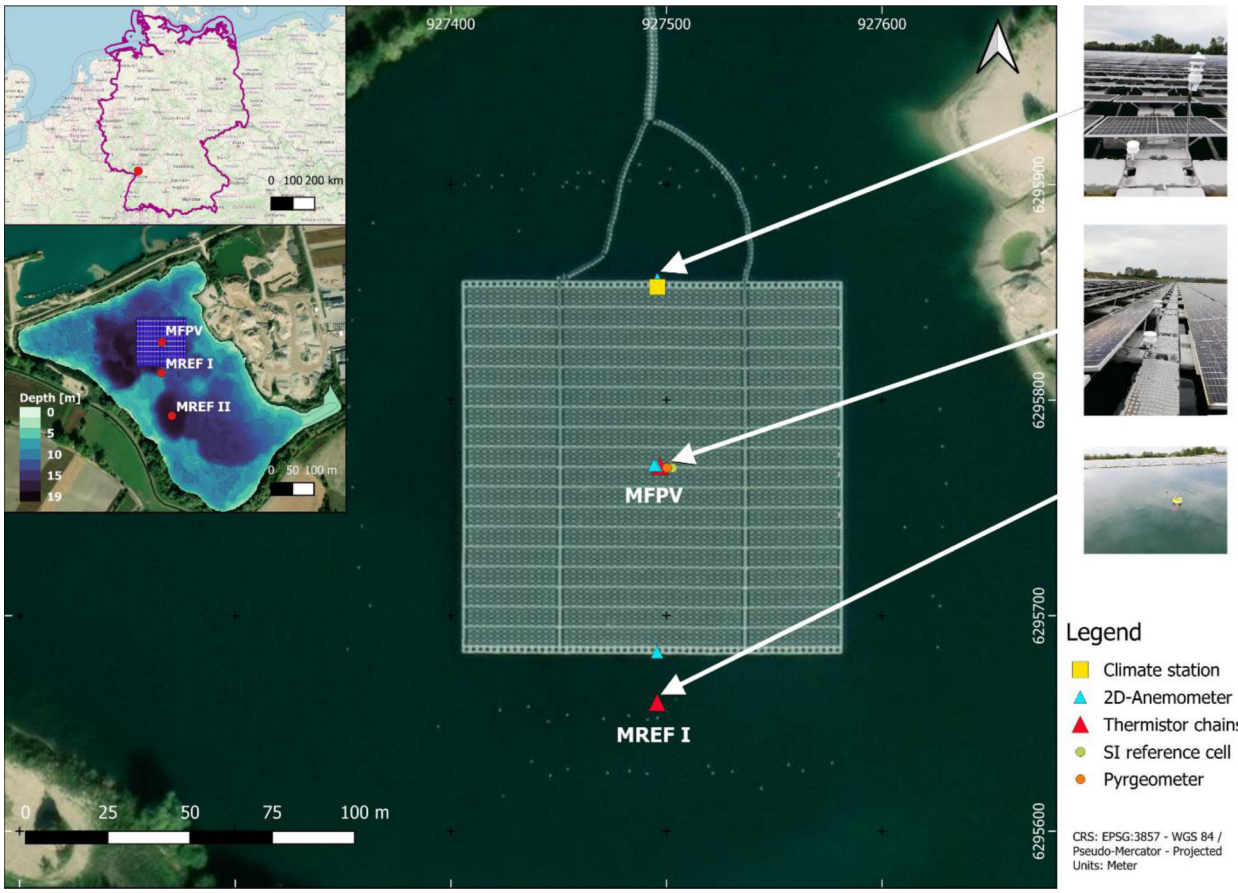

Fig. 1. The monitored floating photovoltaics (FPV) system. The two insets show the location of the studied gravel pit lake in Germany and the measurement points (MFPV, MREFI, MREFII) in the lake. The yellow square indicates the position of the meteorological measuring system.

hydrodynamic modelling to propose ecologically informed regulatory measures. These findings will contribute to a science-based framework for sustainable FPV deployment in aquatic ecosystems.

2 Materials and methods

2.1 Study site

The gravel pit lake near Leimersheim (Lake Leimersheim; latitude 49.123, longitude 8.332) is located in southwest Germany in the Upper Rhine Valley. The mean lake depth is 9.3 m, maximum depth is 19 m, the total lake area is 19 ha, and its water volume is 1.7×10^6 m^3. The lake has no river in- or outflows, and its water level is almost constant, balanced by groundwater inflow. Lake Leimersheim is one of more than 700 gravel pit lakes in the Upper Rhine Valley. Given its depth and hydrological characteristics, Lake Leimersheim is expected to exhibit seasonal thermal stratification, with a thermocline forming at intermediate depths during the summer months. The absence of natural surface inflows or outflows suggests that vertical mixing primarily depends on atmospheric forcing, with full overturn occurring during the colder months. Lake Leimersheim may be characterised as oligotrophic, with low nutrient concentrations and high oxygen availability. Anthropogenic influences, particularly from gravel processing activities, locally affect water clarity and chemical parameters.

The studied FPV system is located in the northern part of the lake (Fig. 1). The first part of the system, with a capacity of 750 kWp, was commissioned in autumn 2020, and the second part, with an additional 750 kWp, in autumn 2021. Both parts have a length and width of 115 m each and consist of 3,744 PV panels arranged over 8% of the lake's total surface area. The total annual electric yield is 1.7 GWh, which is either transferred directly to the adjacent gravel plant or fed into the public grid. The gravel plant can cover 20–30% of its electricity consumption with the electricity from the FPV system. During the study period from 1 January 2023 to 31 July 2024, no excavation took place. The gravel works occasionally resulted in the discharge of sediment-rich process water into the lake.

2.2 Measurement methods

2.2.1 Meteorological data collection

A climate station (WS510-UMB, Lufft) was located at the northern edge of the FPV system to measure global horizontal irradiance (W m^{-2}), wind speed (m s^{-1}), and direction (°), relative humidity (%), atmospheric pressure (hPa), and air temperature (°C) (Fig. 1). Long-wave radiation measurements

Fig. 2. Photograph of the mussel population of a fully submerged floater, taken from the below by the remotely operated underwater vehicle.

were carried out in the centre of the FPV system using a pyrgeometer (SGR3, Kipp & Zonen).

In addition, 2D ultrasonic anemometers (WS200-UMB, Lufft) measured wind speed near the surface. Anemometers at the southern and northern edges of the system were placed at the height of the upper edge of the solar panels, while two anemometers in the centre of the system were installed at different heights. One was mounted 40 cm above the water surface, the other 20 cm above the water surface, with the top edge of the solar panel positioned between the two sensors at 30 cm above the water. The accuracy of the wind direction measurement was ±3°, for wind speed it was ±3% in the range 0–35 m s^{-1}.

By comparing the wind speed at different heights, it was possible to quantify the reduction in wind speed caused by the FPV system. Solar irradiance reduction by FPV was calculated using the Radiance ray-tracing model (Ward, 1994). All sensors were connected using a daisy-chain distributed Modbus architecture, ensuring synchronised and continuous data collection.

2.2.2 Hydrodynamic and temperature monitoring

Water temperature profiles were monitored using thermistor chains (accuracy: ±0.1 °C) to assess thermal stratification and temperature variations beneath the FPV system and in open water. A 10m thermistor chain was deployed beneath the FPV system at its centre (MFPV, Measurement Point Floating PV) to measure water temperature at 50 cm intervals along the vertical profile. An identical chain was installed at a second measurement point located in the open water south of the system (MREF I, Measurement Point Reference I), serving as a reference for comparison (Fig. 1). To obtain a detailed representation of the lake bathymetry, echo sounders were used to record depth profiles, which were then used to generate a depth raster and a hypsographic curve.

2.2.3 Water quality measurements

Water quality was measured using an EXO2 multiparameter probe (YSI Inc. / Xylem Inc.) at MFPV, MREF I and MREF II (Fig. 1). Measurements at MREF I and MREF II were averaged (MREF) and used for comparison with data collected beneath the FPV system at MFPV. During 17 measurement campaigns carried out from 9 May 2023 to 9 July 2024, profile measurements of water temperature, dissolved oxygen, oxygen saturation, specific conductivity, pH, redox potential, nitrate, turbidity, phycocyanin, chlorophyll-*a*, and dissolved organic carbon were conducted at 1m depth intervals down to the lake bottom. Measurements concentrated on the vegetation period and on transition periods of lake mixing regimes. In winter, measurements were taken at larger time intervals during isothermal conditions caused by lake turnover. There was no period with ice coverage.

To further investigate the influence of mussel respiration on oxygen concentrations, two water temperature and dissolved oxygen loggers (miniDOT, PME) were placed at MFPV and MREF I. Both loggers were deployed at a depth of 1 m, recording measurements every 15 minutes with an accuracy of ±0.3 mg l^{-1}. The first measurements were recorded on 5 September 2023, the last on January 9, 2024.

2.2.4 Periphyton and mussel sampling

Mussel colonisation on FPV floaters was also assessed. One floater beneath the FPV panels was removed, and all periphyton was scraped off using hard plastic spatulas. To allow for an estimation of the full population of the FPV system, a remotely operated underwater vehicle (Deep Trekker, DTG3) took pictures of other floaters from below, to ensure that the mussel coverage was comparable between floaters (Fig. 2).

The obtained mussels and periphyton material were sealed and transported to the laboratory, where they were stored in the fridge at −18 °C until further investigation. In the next step, all mussels were counted and the species determined. Each individual was grouped into size classes between <5 mm, 5–10 mm, 11–15 mm, 16–20 mm, and 21–25 mm. Considering the size class distribution of the mussels, 100 mussels of each species were selected, and the shell was

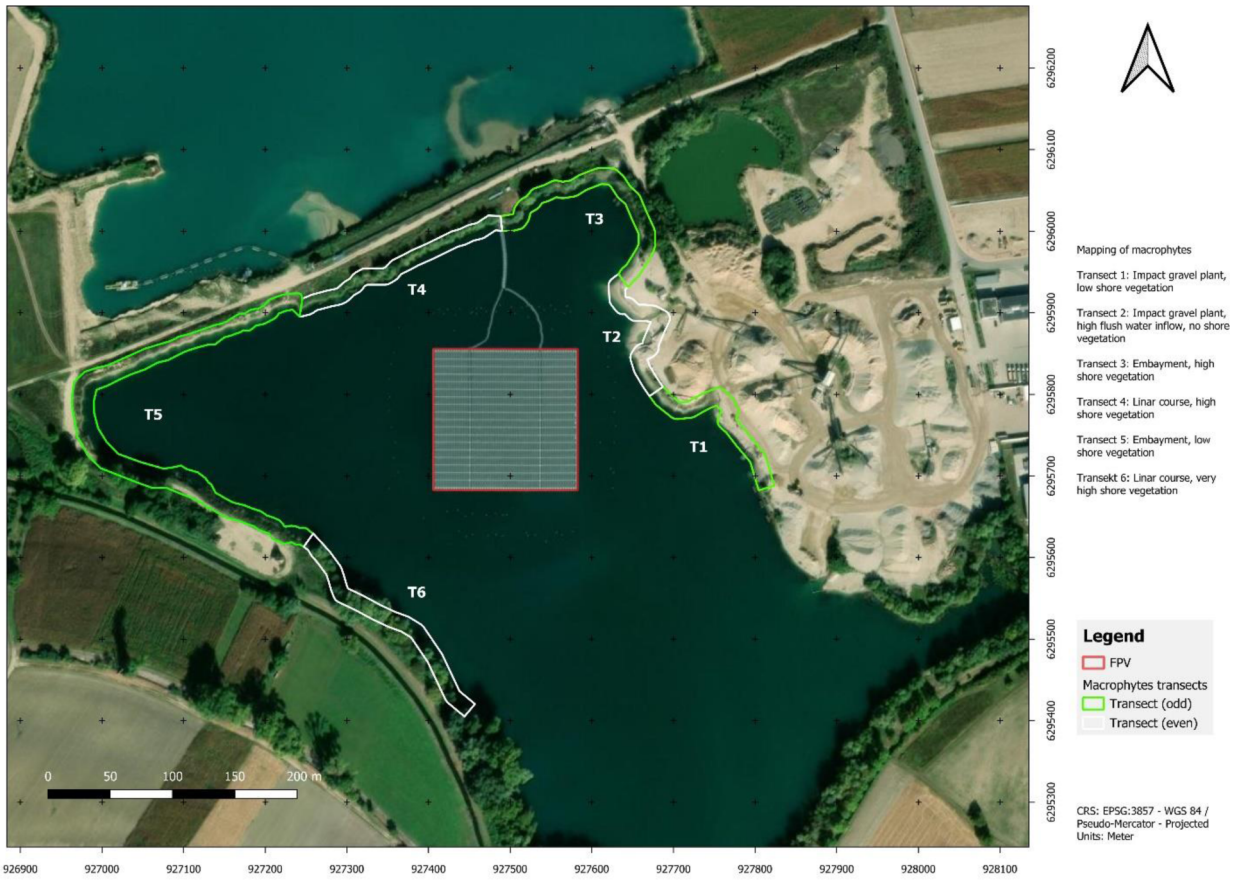

Fig. 3. Boundaries of the macrophyte transects (T1–T6) along the gravel pit lake shoreline. The floating photovoltaic (FPV) system is highlighted with a red rectangle. Coordinates are given in metres.

separated from the body. Fresh and dry weight was measured before and after drying at 105 °C. The dry material was then ground and analysed for phosphorus content.

To evaluate the overall mussel filtration performance, an effective clearance rate of 41.95 ml ind^{-1} h^{-1} was derived from literature values (Yu and Culver, 2001), with a range between 15.3 mL ind^{-1} h^{-1} and 68.6 mL ind^{-1} h^{-1}. Diggins (2001) reported 309 mL ind^{-1} h^{-1} for quagga mussels and 226 mL ind^{-1} h^{-1} for zebra mussels. Consequently, the derived estimate represents a conservative assumption for a mixed mussel population. This estimate enabled a comparison of the total filtered water volume relative to the overall lake volume.

2.2.5 Macrophyte sampling

To assess the suitability of current FPV regulations and to propose ecologically informed regulatory measures, macrophyte sampling was conducted. In Germany, the construction of FPV installations is regulated by the Water Resources Act (WHG), a national legal framework for water protection and management. This law mandates a 40 m distance from the shoreline for FPV systems, to protect littoral zones, where macrophyte communities are typically found.

The size of the littoral zone can vary significantly within a lake and may also depend on the lake type. While the WHG serves as a national German law, the European Water Framework Directive (WFD) provides an overarching framework for ecological water quality. The WFD establishes standardised ecological quality criteria and specific assessment methods for aquatic ecosystems, including macrophytes, to ensure a harmonised evaluation across Europe. Accordingly, the macrophyte investigation in this study was carried out in July 2024, following the WFD assessment guidelines for macrophytes in lakes (van de Weyer and Stelzer, 2021). For this purpose, the shoreline area around the FPV system was divided into six transects (Fig. 3).

The transects were of similar length but differed in shoreline characteristics. Transects 1 (T1) and 2 (T2) were located near the gravel plant, with T2 receiving water from the gravel washing process. T3 extended along a bay and had dense riparian vegetation, while T4 was linear, with a south-eastern exposure. T3 and T4 were separated by the FPV system's floating power cable. T5 had recently been excavated, resulting in sparse vegetation. T6 was linear, similar to T4, and exposed to the north-east. It had the densest riparian vegetation, including overhanging trees. Macrophyte sampling was conducted at depths of 0.0–1.0 m, 1.1–2.0 m, 2.1–4.0 m, and >4.0 m by a team of two divers and a protocol writer.

In addition to transect sampling, a cross-sectional control dive beneath the FPV system identified potential macrophyte communities. A field protocol recorded shoreline conditions and species abundance classified on a scale from 1 (very rare)

to 5 (abundant). The lower macrophyte limit (LML) was determined and compared with multibeam echosounder data. The LML describes the maximum depth at which submerged macrophytes can grow under specific light conditions, serving as an ecological indicator of water transparency and habitat suitability.

A Helix 7 SI GPS G4 sonar (Humminbird, USA) was used to map macrophyte distribution. The lake was evaluated based on WFD metrics, including structure, number of habitat-typical species, and LML. Lake type classification considered stratification, calcium content, altitude, and catchment size. Ecological status was assessed based on habitat-typical vegetation cover (%), species richness, and LML. This was evaluated using WFD reference tables (van de Weyer and Stelzer, 2021), providing an overall rating of the lake's ecological condition.

2.3 Statistical analysis

For measurements obtained with the EXO2 multiparameter probe, mean values were calculated at corresponding depths for MFPV and MREF, and deviations at MFPV were assessed relative to MREF. *t*-tests were conducted for all parameters, and the observed deviations were compared with measurement uncertainties provided by the manufacturer. To represent FPV in hydrodynamic models, mean values with standard deviations and statistical significance were calculated for reductions in wind and solar irradiance, as well as for light extinction. For the mussel distribution, a χ^2 test was applied to assess the statistical significance of the differences in species composition across size classes.

2.4 Hydrodynamic and ecological modelling

2.4.1 Model Configuration

The General Lake Model (GLM–AED2, V3.0.0) was used to model FPV-induced changes and predict long-term effects under high FPV coverage. GLM uses a Lagrangian grid and energy balance approach for surface mixing (Hipsey *et al.*, 2019), while AED2 simulates aquatic ecodynamics, including nutrient cycling and geochemistry (Hipsey, 2022).

For comparison, Delft3D-FLOW was used as an alternative model for unsteady, 3D flows simulations, incorporating meteorological forcing, and density variations (Deltares, 2024). Both models used the same meteorological input — initially from NASA's POWER project (1 January 2023 – 12 August 2023; NASA, 2023) and thereafter from a climate station on the FPV system. Variables included shortwave and longwave radiation, air temperature, wind speed/direction (direction only for Delft3D-FLOW), relative humidity, rain, and snow. As no precipitation data were collected on-site, values were taken from a nearby German Meteorological Service station (ID: 05906). Reductions in solar irradiance and wind, simulated via a ray-tracing model, along with wind measurements, were integrated into both models.

For lake bathymetry, Delft3D-FLOW utilised a depth raster from echo sounder data, while GLM-AED2 applied a hypsographic curve. Given the same initial conditions (water temperature and water level), both models were calibrated using depth profile measurements from reference points (MREF I, MREF II), with GLM-AED2 employing the CMA-ES method (Varelas *et al.*, 2018). Calibration and validation periods were split by a ratio of 2:1, and the total modelling period was from 1 January 2023 to 30 June 2024. Model performance was evaluated using Root Mean Square Error (RMSE), Nash–Sutcliffe model efficiency coefficient (NSE) and Kling–Gupta efficiency (KGE).

2.4.2 FPV coverage scenarios

Simulations were conducted for FPV coverage scenarios of 8% —correspond to the existing FPV system—as well as 15%, 30%, 45%, and 90%. In Germany, the legal maximum FPV coverage is 15%, while 90% represents the technical limit of FPV installations (Wirth *et al.*, 2021). Globally, FPV installations typically cover between 10% and 45% of a water surface, with higher coverage being less common due to environmental and technical constraints (Xia *et al.*, 2023; Nobre *et al.*, 2024). The selected coverage scenarios therefore reflect both current regulatory limits and potential future expansion.

Model simulations were evaluated by comparing key hydrodynamic metrics, including lake surface water temperature, Schmidt stability, and thermocline depth. Schmidt stability represents the energy required to mix the entire water column to a uniform temperature (Schmidt, 1928; Idso, 1973). If Schmidt stability is positive, stratification and thermocline formation can be assumed. Thermocline depth was calculated as the depth at which the maximum density gradient occurs, provided water temperature exceeded 4.0 °C and density difference between surface and bottom layers was greater than 0.1 kg m^{-3} (Ladwig et al., 2021).

Both Schmidt stability and thermocline depth were computed using the rLakeAnalyzer package (Winslow *et al.*, 2018). Additionally, the trophic state index (TSI; Carlson, 1977) was simulated using GLM-AED2 to assess potential shifts in lake productivity under different FPV scenarios:

$$TSI(Chl) = 10\left(6 - \frac{2.04 - 0.68\,ln(Chl)}{\ln 2}\right) \quad (1)$$

where Chl is the chlorophyll-*a* concentration (μg l^{-1}) at the water surface. TSI values range from 0 to 100, with each major interval (10, 20, 30, *etc.*) representing a doubling in algal biomass.

2.4.3 Macrophyte distribution and FPV coverage optimisation

By comparing current LML with theoretical LML under the Trophic Reference State (TRS), GLM-AED2 provided a spatial assessment of macrophyte expansion potential and its implications for FPV siting. TRS represents the ecological baseline of the lake in an undisturbed state, where macrophytes could extend deeper due to improved water quality and reduced anthropogenic pressure. Macrophyte growth was considered light-limited, with a threshold set at 1% of surface irradiance (Schwoerbel and Brendelberger, 2013; Liu *et al.*, 2016). The model also accounted for mussel filtration effects on water clarity, as colonies attached to the FPV substructure

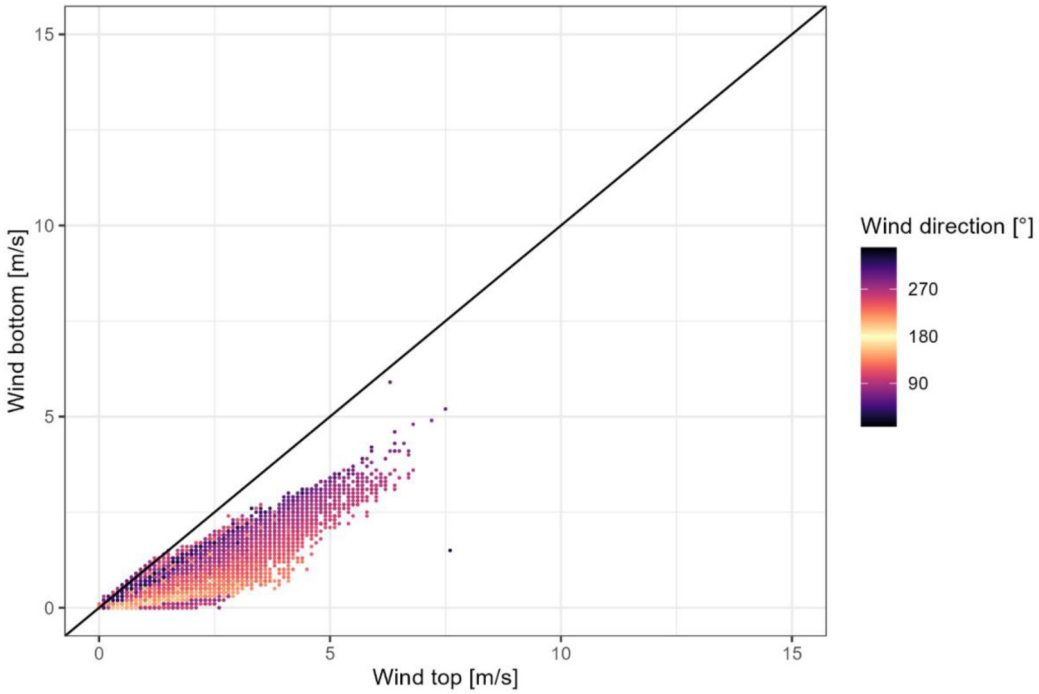

Fig. 4. Comparison of wind speed measured above (*Wind top*) and below (*Wind bottom*) the PV modules, depending on the wind direction.

improve light penetration, potentially expanding macrophyte habitats and influencing FPV placement constraints. First, the macrophyte-free zone under TRS conditions was determined. Then, FPV coverage scenarios were simulated for 8%, 15%, 30%, 45% and extended to cover the entire macrophyte-free zone. To assess the maximum FPV coverage in a restored ecosystem, the model simulated scenarios with and without mussel filtration, quantifying LML shifts and the corresponding reduction in the macrophyte-free zone. Mussel filtration effects were incorporated into the GLM-AED2 simulation by adjusting the light extinction coefficient (k_w), which can be calculated using measurements of light intensity or turbidity at different depths:

$$k_w = \frac{1}{z}\ln\left(\frac{I_0}{I_z}\right) \tag{2}$$

where I_0 is the light intensity at reference depth directly below the water surface, and I_z is the light intensity at distance z below reference depth (Schwoerbel and Brendelberger, 2013). Assuming proportionality of light intensity and turbidity, k_w was determined by:

$$k_w = \left(\frac{ln}{z}\right) \times \left(\frac{Turb}{z}\right) \tag{3}$$

where *ln* is the natural logarithm and Turb is turbidity in Nephelometric Turbidity Units (NTU). This analysis is particularly relevant for FPV deployment beyond the excavation phase, as it highlights the importance of integrating ecological restoration objectives into site selection and long-term lake management.

3 Results

3.1 Meteorological forcing and FPV-induced wind and irradiance reduction

Continuous wind measurements conducted at the FPV system revealed a substantial wind reduction of 57% (±22.6%) beneath the FPV system ($p < 2.2 \times 10^{-16}$). This reduction increased with rising wind speeds, indicating a stronger reduction at higher wind velocities. Southern winds, which directly impinged upon the southward-oriented foundations of the array, resulted in a more substantial wind reduction compared to northern winds (Fig. 4).

Radiance simulations indicated an 88% (±10.3%) reduction in solar irradiance reaching the water body beneath the system ($p < 2.2 \times 10^{-16}$). While some areas—particularly along cable routes and at the array's edges—experienced minimal or no shading, a high degree of shading was observed under the modules and the substructure. This reduction in light availability was accompanied by a 36% (±31.1%) decrease in k_w, as derived from turbidity measurements ($p = 0.0062$). These measured reductions, along with wind reduction, were used to represent the FPV system in the models through coverage-based adjustments of model parameters (Tab. 1).

3.2 Water quality effects under FPV coverage

There was no significant difference in water temperature between MFPV and MREF ($p = 0.856$; Fig. 5). In contrast, a significant decrease in both dissolved oxygen concentrations (ΔDO, $p = 0.011$) and oxygen saturation (ΔDO Sat, $p = 0.01$) was observed beneath the FPV system. Nitrate concentrations

Table 1. Parameters adjusted to represent FPV in GLM-AED2 and Delft3D-FLOW.

Parameter	Without FPV	With FPV	Deviation (%)
Scaling factor for shortwave radiation (*sw_factor*)	1.0	0.12	88
Scaling factor for wind speed (*wind_factor*)	1.0	0.43	57
Light extinction coefficient (k_w)	0.383	0.244	36

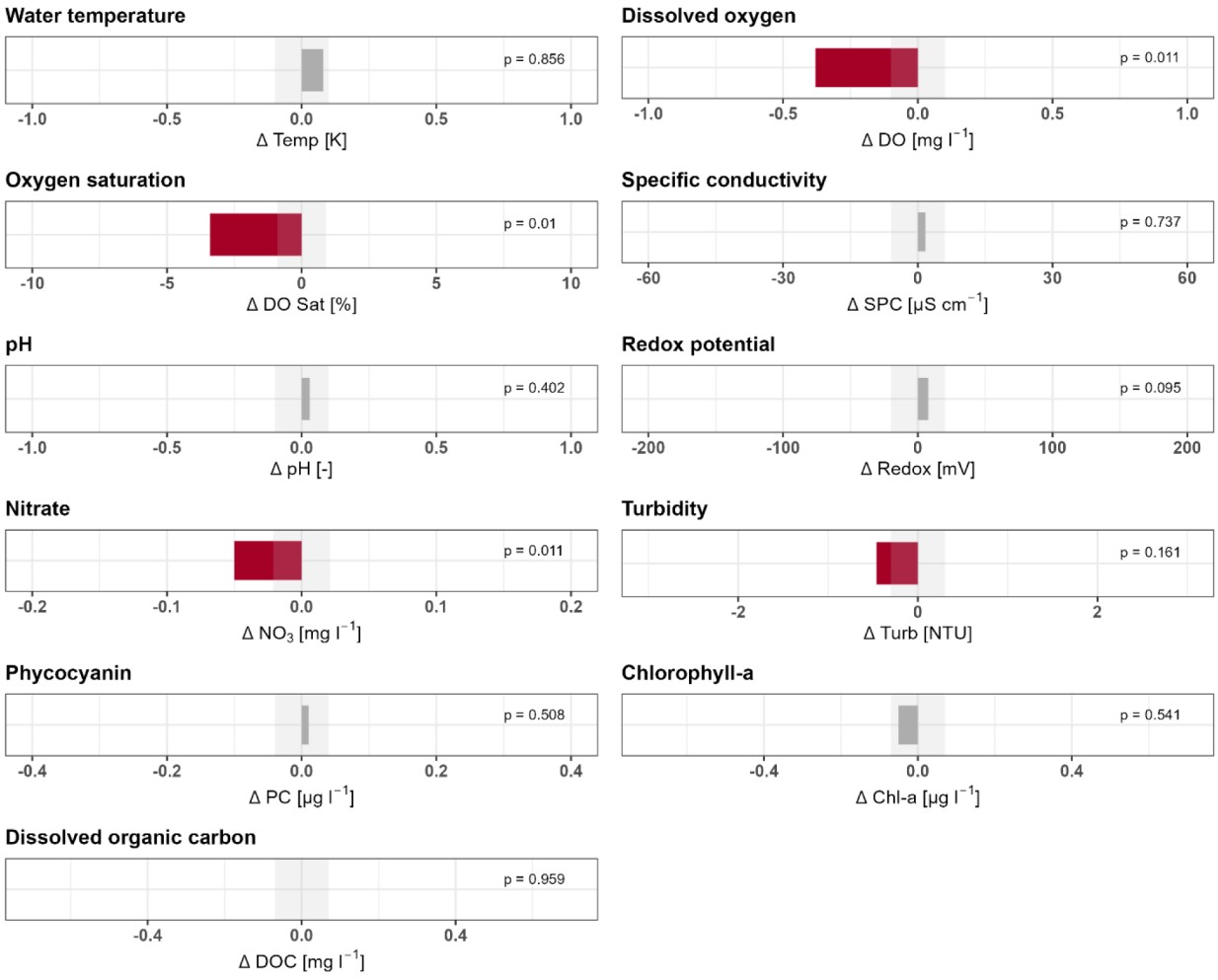

Fig. 5. Deviations of measured parameters between MFPV and MREF. MREF is defined as the mean of MREFI and MREFII. The grey shaded area represents measurement uncertainty; if a deviation falls within this range, the corresponding bar is coloured dark grey. Red bars indicate deviations that exceed the measurement uncertainty. Statistical significance is determined using *p*-values, which are displayed in the upper right corner of each plot, with $p < 0.05$ indicating statistical significance.

also exhibited a significant reduction (ΔNO_3, $p = 0.011$). Turbidity showed a decreasing trend ($p = 0.161$), with deviations exceeding the measurement uncertainty, indicating a measurable effect of the FPV system on water clarity. Other parameters—including specific conductivity ($p = 0.737$), pH ($p = 0.402$), redox potential ($p = 0.095$), phycocyanin ($p = 0.508$), chlorophyll-*a* ($p = 0.541$), and dissolved organic carbon ($p = 0.959$)—showed no significant differences between MFPV and MREF, with deviations falling within the range of measurement uncertainty. The relatively low concentrations of chlorophyll-*a* (1.08 µg l^{-1} at MREF) and nitrate (0.21 mg l^{-1} at MREF), along with the calcareous sediment signature inferred from the specific conductivity (594 µS cm^{-1}) and pH (8.14) values, are characteristic of an oligotrophic trophic state, which aligns with the expected water quality of the gravel pit lake.

3.3 Mussel colonisation and filtration impact

3.3.1 Mussel colonisation and population density

Mussel density on the hard substrate with permanent water coverage was so high that periphyton assessment was impossible. The coverage was completely dominated by the mussels. On half a floater, 1,771 individuals were counted,

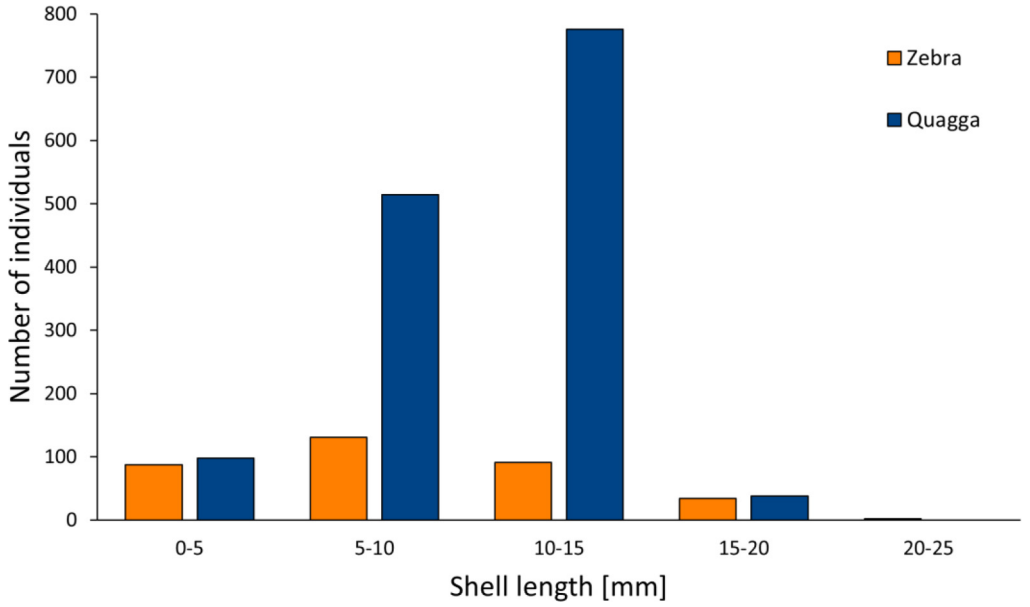

Fig. 6. Distribution of shell length values of zebra (*Dreissena polymorpha*) and quagga mussel (*Dreissena rostriformis bugensis*) on one half of a floater.

with quagga mussels (80.5%; 1,426) outnumbering zebra mussels (19.5%; 345). Shell length analysis showed significant quagga dominance (p-value = 2.01×10^{-37}), particularly in the 5–10 and 15–20 mm size classes (Fig. 6).

The sampled floater contained approximately 3,500 mussels. Since it was only 50% submerged, fully submerged floaters carrying PV panels were estimated to host around 7,000 mussels each. Considering that approximately 10% of the floaters (walkways) have reduced weight and reduced a specific water-contact-surface, the total mussel population across 3,952 floaters was estimated at 26.3 million.

3.3.2 Effects of mussel filtration on water quality

Oxygen concentrations varied significantly between sites, with a daily amplitude of up to 7 mg l^{-1} at MREF I, which remained below 0.8 mg l^{-1} at MFPV. Beneath low or moderate global horizontal irradiance, dissolved oxygen was reduced under FPV (Fig. 7, zoom window 1). During periods of warm and stable weather, dissolved oxygen fluctuations in the open water were significantly higher than below the FPV (Fig. 7, zoom window 2).

To estimate the phosphorus removal potential of the mussel population on the FPV system, various parameters were measured and calculated, including dry weight, phosphorus content, and filtration capacity. A dry weight of 0.589 g and 0.554 g was measured for 100 individuals of quagga and zebra mussels respectively. The average phosphorus content was 10.38 mg g^{-1}, binding 414 mg of phosphorus per floater. Shells contained 0.16 mg g^{-1} phosphorus, with a dry weight of 6.3 g (quagga) and 8.3 g (zebra) per 100 shells, binding 81.8 mg phosphorus per floater. Across all floaters, mussel bodies stored 1.64 kg of phosphorus, and shells 0.32 kg. The calculated effective clearance rate for mussel population attached to the FPV system was 26,460 m^3 d^{-1}, filtering 1.5% of the total lake volume or 3.1% of the epilimnion per day.

3.4 Macrophyte distribution and ecological lake condition

A total of 15 macrophyte species were identified during the diving surveys in T1–T6 (Fig. 8).

Species diversity was highest in T3 and T4, with up to ten species identified (Fig. 9). Fewer species were observed in other transects, including T2 and T6. Macrophyte abundance peaked at 1–2 m depth but was lower at 0–1 m. At depths exceeding 4 m, abundance declined, with *Ceratophyllum demersum* and *Potamogeton lucens* dominating, while *Myriophyllum spicatum* prevailed in shallower areas. *Chara virgata* (coverage ratio = 0.5%) was the only habitat-typical species, according to the WFD assessment for this lake type. Others, *e.g., Nitella spp.*, *Nitellopsis obtusa* and *Tolypella spp.*, were missing.

Based on stratification patterns, water quality (SPC and pH), geographical location, and the absence of natural surface inflows, the lake was categorised as a stratified, calcium-rich lowland lake with a small catchment (type 13) and an oligotrophic TRS. Mean LML of 5.25 m (±0.52 m), along with the cover ratio and habitat-typical species count, classified the lake's ecological condition as insufficient (Tab. 2).

Macrophytes were only observed in nearshore areas, with no growth detected beneath the FPV system. This corresponds with current LML of 5.25 m, suggesting that bathymetric constraints, rather than direct FPV shading, limited macrophyte growth below the system.

3.5 Hydrodynamic modelling performance and FPV impact analysis

3.5.1 Model calibration and validation

Both GLM-AED2 and Delft3D-FLOW demonstrated high performance during the calibration period, based on averaged measurements from MREFI and MREFII, achieving RMSE

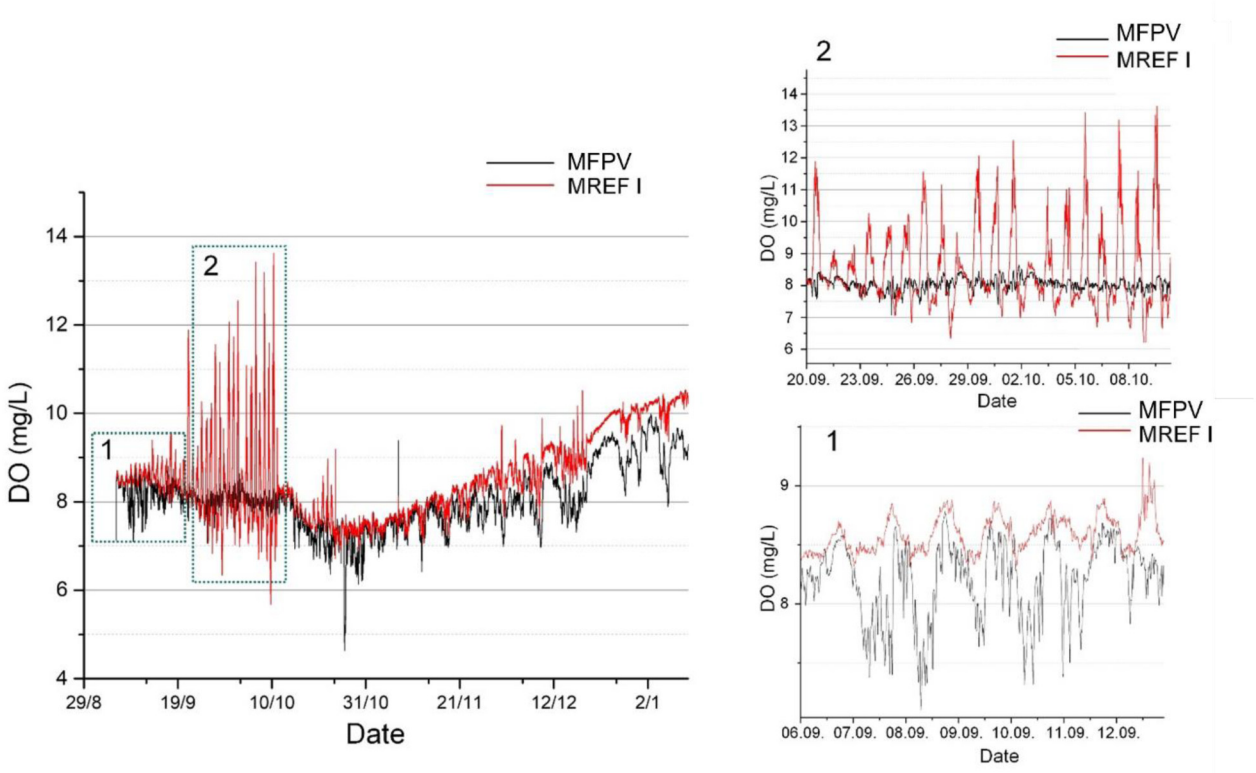

Fig. 7. Dissolved oxygen concentrations at 1 metre depth below the FPV and in open water (MREF I) from 5 September 2023 to 9 January 2024, as measured by the miniDOT loggers.

values below 1 °C and NSE values exceeding 0.9 for water temperature profiles (Tab. 3).

Using the same metrics, modelling results were evaluated for the entire simulation period, both at the reference and below FPV, assuming the current FPV coverage of 8%. Both models achieved NSE values above 0.6 and RMSE between 1 °C and 2 °C, indicating a satisfactory representation of the system (Tab. 4).

3.5.2 FPV coverage effects on stratification, mixing, and trophic state

Simulated water temperature profiles at various depths were compared with field data for both models (Fig. 10). While both models captured overall water temperature trends, they differed in detail. GLM-AED2 predicted smaller fluctuations in surface water temperatures, whereas Delft3D-FLOW overestimated surface temperatures, especially during summer 2023. Both models performed better for epilimnetic than hypolimnetic temperatures. GLM-AED2 predicted higher bottom temperatures at the onset of stratification, while Delft3D-FLOW tended to underestimate them. The formation of inverse stratification in winter was more pronounced in the Delft3D-FLOW simulation.

Both models accurately reproduced thermal stratification during summer (Fig. 11). At an FPV coverage of 45%, stratification became more unstable in both models, suggesting an upward shift in the thermocline.

With increasing FPV coverage, both models showed a general decline in lake surface water temperature (Fig. 12). For low FPV occupancies (≤15%), temperature reductions remained moderate, with differences of approximately 1 °C compared to the baseline scenario. For 90% FPV coverage, GLM-AED2 simulated a 3.6 °C temperature reduction, whereas Delft3D-FLOW predicted a reduction of 7.2 °C.

Schmidt stability, an indicator of stratification strength, decreased at high FPV coverage in both models. In Delft3D-FLOW, Schmidt stability initially increased at 15% and 30% FPV coverage, before sharply declining from 45% and onwards, indicating a mid-range peak in stratification intensity. In contrast, GLM-AED2 exhibited a steady decline already up to 45%, followed by a more pronounced drop.

Despite these differences, both models converged to similar stability levels for 90% FPV coverage, suggesting that extensive FPV deployment results in comparable reductions in stratification. This weakening was also evident in reduced thermocline depths. While Delft3D-FLOW consistently simulated a shallower thermocline than GLM-AED2, both models showed notable decreases in thermocline depth beyond 30% FPV coverage. The TSI, simulated only by GLM-AED2, declined with increasing FPV coverage, suggesting potential reductions in lake productivity. This trend aligned with observed reductions in lake surface water temperature and increased shading, both of which constrain primary production. Compared to the baseline, TSI decreased by approximately 20% at 30% FPV coverage and by 60% at 90% coverage.

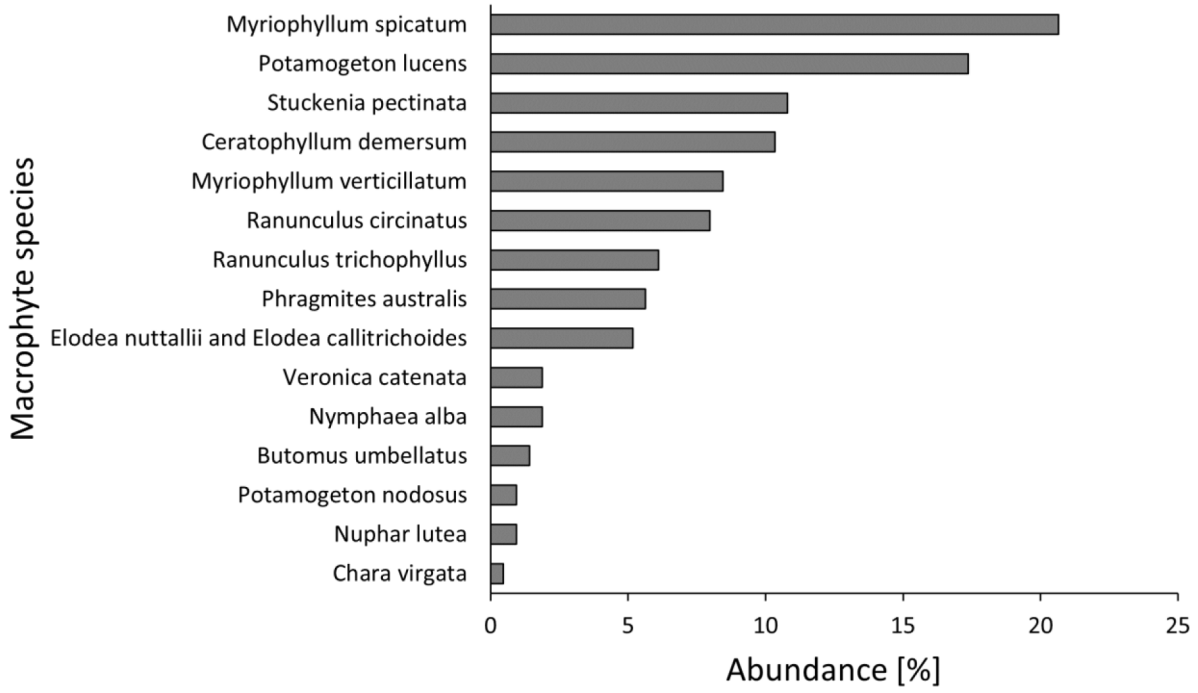

Fig. 8. Abundance of the macrophyte species found within the six macrophyte transects along the shore of the gravel pit lake (T1–T6).

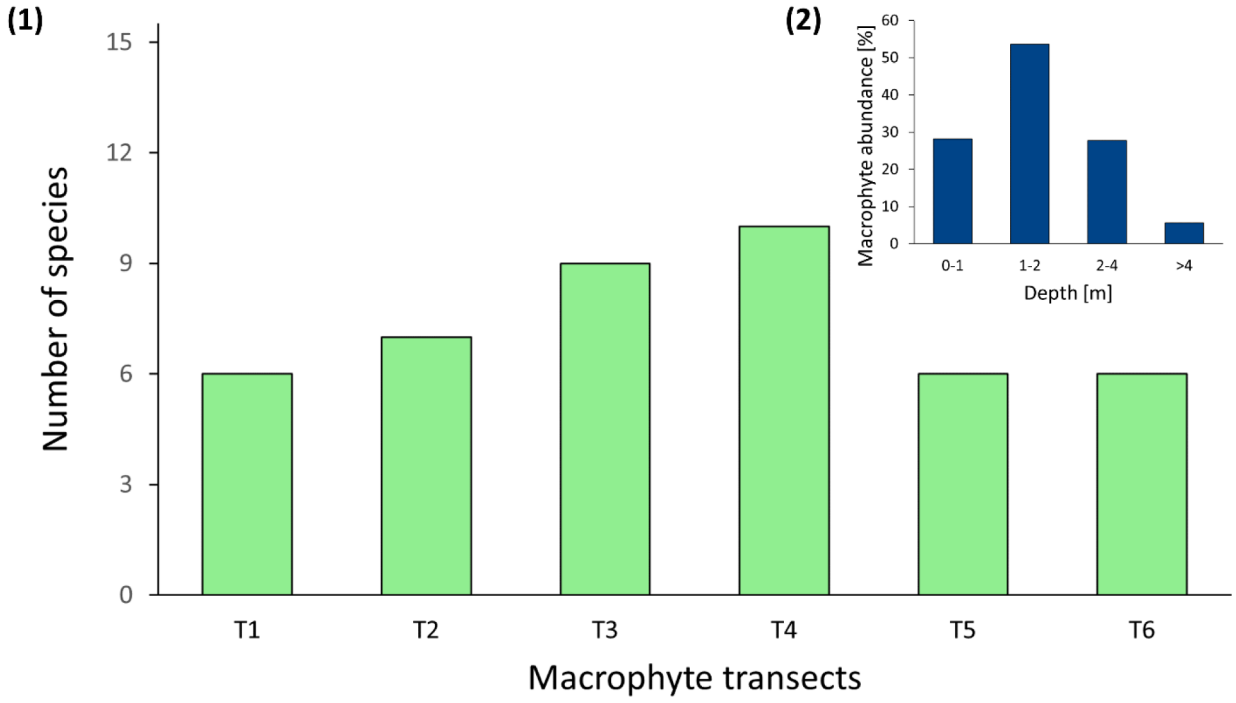

Fig. 9. (1) Number of species found in six macrophyte transects (T1–T6, Fig 3); (2) distribution of macrophyte abundance in relation to water depth.

3.5.3 Modelling mussel filtration effects on lower macrophyte limit

To assess the impact of mussel filtration on macrophyte expansion, GLM-AED2 simulations were used to estimate shifts in the lower macrophyte limit (LML) under varying FPV coverage scenarios (Fig. 13). The current LML-based macrophyte distribution was expanded by the WFD-defined theoretical LML for good (oligotrophic) lake conditions. The latter LML formed a potential contact zone northeast of the FPV system. The maximum observed shoreline distance to the current LML was 35 m. In contrast, the shoreline distance to theoretical LML

Table 2. Quality levels (very good, good, moderate, insufficient, bad) for ecological evaluation according to the European Water Framework Directive (WFD). The quality levels determined by the study were as follows: cover ratio of habitat-typical vegetation – bad, habitat-typical species – bad, mean lower macrophyte limit – moderate.

TRS	Very good	Good	Moderate	Insufficient	Bad
Cover ratio of habitat-typical vegetation	>75%	50–75%	10–50%	5–10%	< 5%
Habitat-typical species	>9	6–9	4–5	2–3	1–0
Mean lower macrophyte limit	>10 m	>6.5–10.0 m	>5.0–6.5 m	2.5–5.0 m	<2.5 m

Table 3. Calibration and validation results for GLM-AED2 and Delft3D-FLOW water temperature simulations. Model performance is given by Root Mean Square Error (RMSE), Nash-Sutcliffe model efficiency coefficient (NSE) and Kling-Gupta efficiency (KGE).

Model	Calibration period			Validation period		
	RMSE [°C]	NSE [–]	KGE [–]	RMSE [°C]	NSE [–]	KGE [–]
GLM-AED2	0.77	0.92	0.83	2.41	0.61	0.79
Delft3D	0.71	0.95	0.59	2.91	0.58	0.5

Table 4. Total period results for GLM-AED2 and Delft3D simulations for the reference and FPV (actual coverage, 8%).

Model	Reference			FPV		
	RMSE [°C]	NSE [–]	KGE [–]	RMSE [°C]	NSE [–]	KGE [–]
GLM-AED2	1.94	0.72	0.84	1.5	0.95	0.87
Delft3D	1.78	0.77	0.52	2.63	0.69	0.47

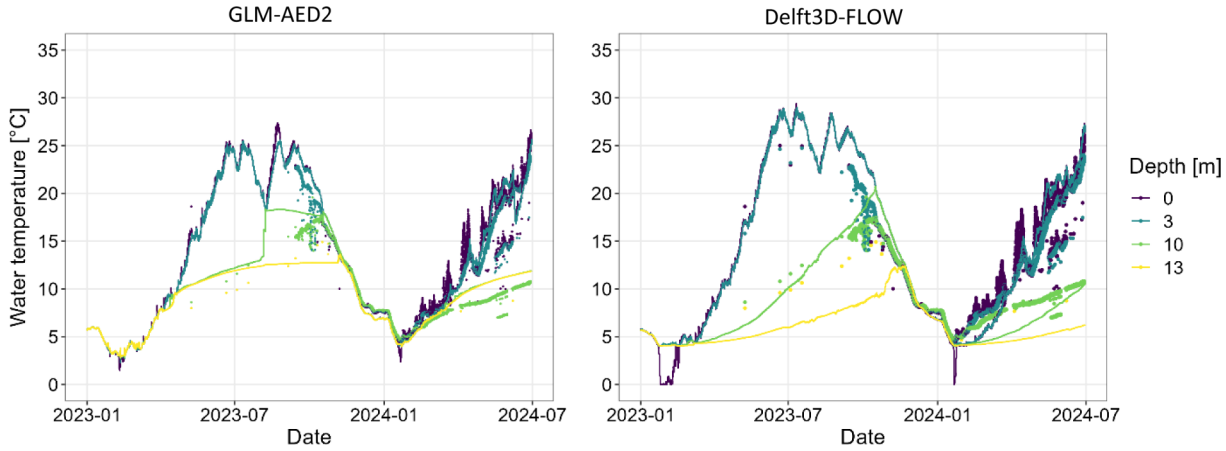

Fig. 10. Comparison of modelled water temperature at different depths for both models (lines), in relation to measured values (dots), below the FPV system with 8% lake coverage.

reached up to 200 m, indicating a heterogeneous distribution based on lake morphology. The GLM-AED2 was calibrated to this theoretical LML, defining the macrophyte-free zone as 58% of the total lake area. Including mussel filtration into the model simulations resulted in LML shifts of 0.32, 0.61, 1.21, 1.99 and 3.07 m for 8%, 15%, 30%, 45%, and 58% FPV coverage, respectively. With increasing water clarity, macrophyte expansion reduced the macrophyte-free zone from 58% down to 46%.

4 Discussion

4.1 Measured effects of FPV on water quality

The overall impact of the installed FPV system on water quality was limited, with considerable reductions observed only in dissolved oxygen, nitrate concentrations, and turbidity. A statistically significant decrease in dissolved oxygen (ΔDO, $p = 0.011$) and oxygen saturation (ΔDO Sat, $p = 0.01$) was recorded beneath the FPV system, along with a reduction in nitrate concentrations (ΔNO_3, $p = 0.011$). De Lima *et al.* (2021) reported oxygen reductions of 1.1–1.7 mg l^{-1} beneath an FPV system covering 30% of a lake in the Netherlands, while Château *et al.* (2019) reported a reduction of 0.86 to 0.89 mg l^{-1} beneath a 40% FPV coverage system in Taiwan.

In comparison, our study—focusing on a system covering 8% of the lake—observed a smaller average reduction of 0.38 mg l^{-1}, suggesting a negative correlation between oxygen concentration and FPV coverage. Additionally, both Château *et al.* (2019) and Li *et al.* (2023) found significant reductions in nitrate concentrations beneath FPV systems,

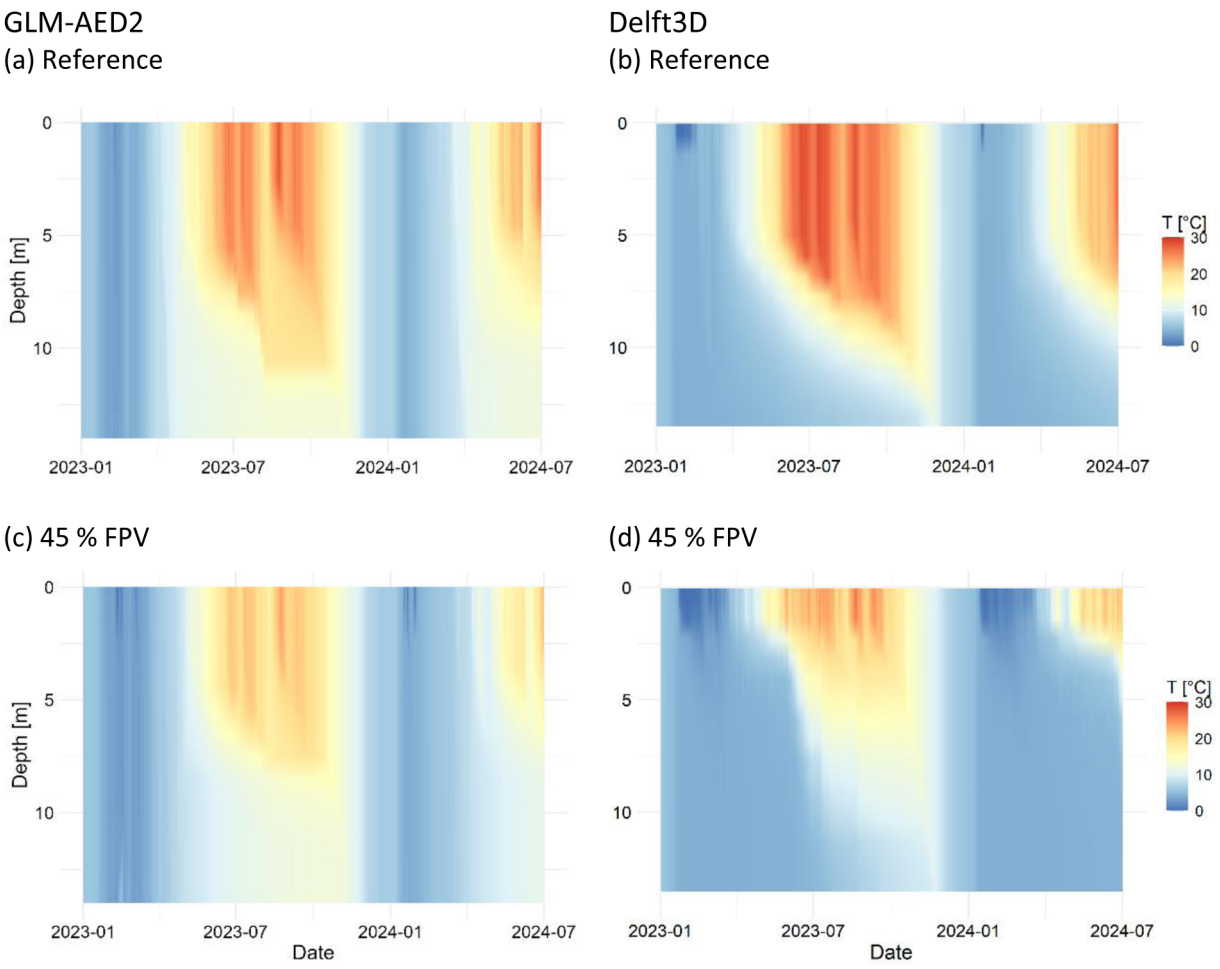

Fig. 11. (a, b) GLM-AED2 and Delft3D-FLOW water temperature profiles at MFPV during the simulation period (January 2023 to July 2024) for the reference scenario; (c, d) water temperature profiles at MFPV with 45% FPV coverage for each model.

which is consistent with our results. Other water quality parameters in our study—including water temperature, pH, specific conductivity, and chlorophyll-*a*—showed no significant differences between MFPV and MREF, indicating that the FPV system's impact on overall water quality was minimal.

4.2 FPV substructure as a new mussel habitat

FPV substructures provide habitat for sessile organisms, particularly mussels, which filter nutrients and suspended solids – potentially reinforcing the shift towards oligotrophic conditions. These mussels filter particles from 1.5 to >40 µm (Lei *et al.*, 1996; Roditi *et al.*, 1996). On our FPV system, nearly 2 kg of phosphorus was bound in mussel biomass, reducing its availability to phytoplankton and macrophytes, which could alter species composition. Drops in oxygen at MFPV compared to MREFI during low solar irradiance (Fig. 7) may indicate higher respiration rates and increased biological activity from periphyton and mussels. In contrast, pronounced diurnal oxygen fluctuations under high solar irradiance at MREFI suggest enhanced primary production at MREF I, while limited variation at MFPV suggested lower net oxygen production. Reduced photosynthesis under FPV can be expected, since shading limits autotrophic metabolism —potentially affecting oxygen dynamics, nutrient cycling, and ecosystem functioning. Mussels typically inhabit benthic zones, but colonising FPV substructures places them in the epilimnion—a warmer, oxygen-rich layer—potentially affecting growth, reproduction, and feeding. This might promote the spread of invasive species but also affect FPV buoyancy. In lakes with a high presence of invasive mussel species, the additional colonisation on the FPV system may be mitigated through designs that minimise float–water contact.

Further manage mussel colonisation, strategies might include encouraging native species – particularly those at risk –or establishing edible mussel farms (Haag and Williams, 2014; Dalderup *et al.*, 2020; Benjamins *et al.*, 2024). Active mussel harvesting could further counteract eutrophication by removing excess nutrients (Soto and Mena, 1999; Gren *et al.*, 2009; Petersen *et al.*, 2014). By reducing nutrient availability, mussel filtration on FPV structures may reinforce FPV-induced effects and contribute to a long-term shift towards oligotrophic conditions, mitigating eutrophication in nutrient-rich lakes. Further research is needed here to fully understand ecological effects of colonised FPV systems.

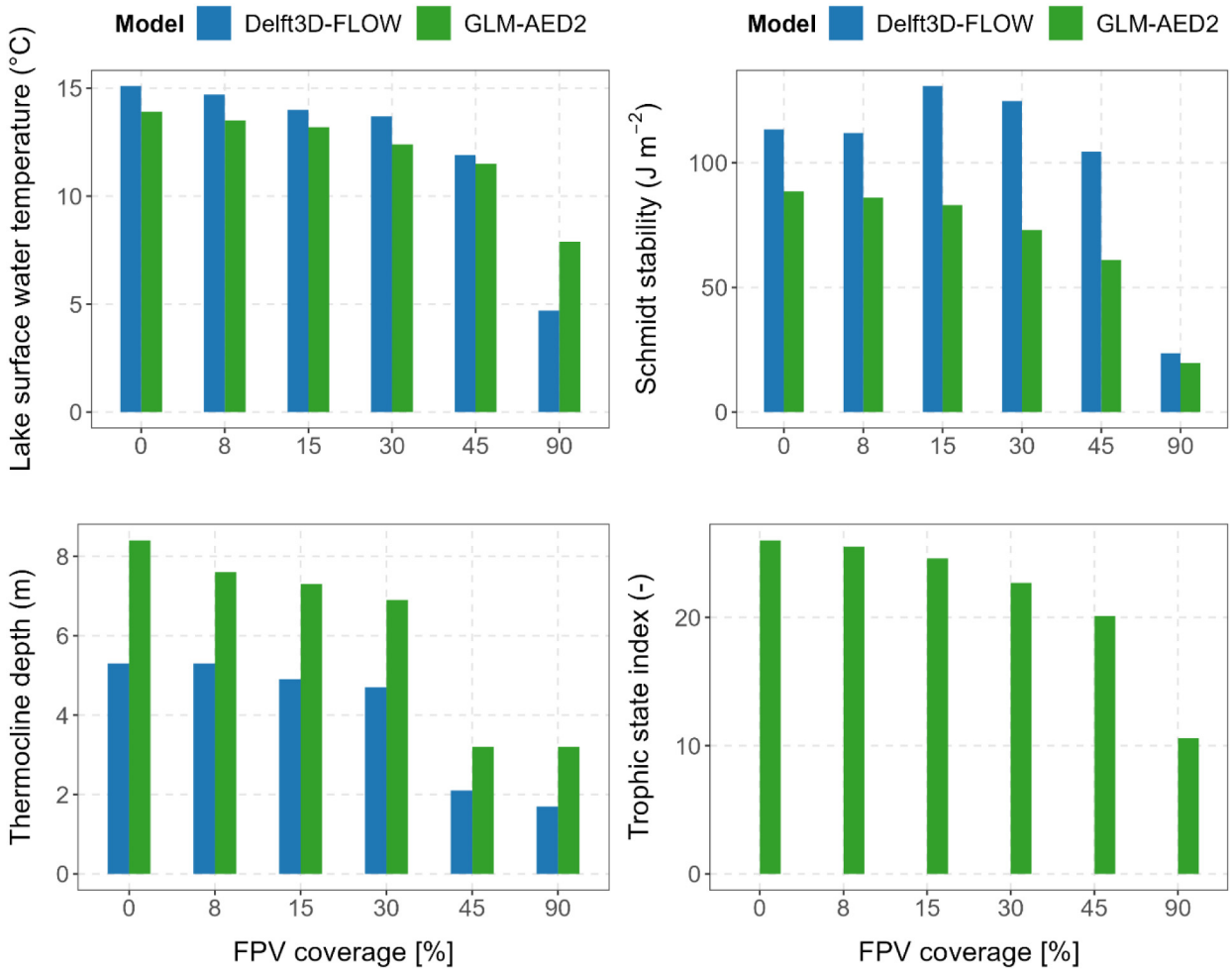

Fig. 12. Simulated impact of FPV coverage on mean lake surface water temperature, Schmidt stability, thermocline depth, and Trophic State Index (TSI) as calculated by GLM-AED2 (green) and Delft3D-FLOW (blue).

4.3 Macrophyte dynamics and limiting factors in FPV-integrated lakes

The highest species diversity was observed in T3 and T4, with up to ten species identified (Fig. 9), likely due to their south-facing location and relatively undisturbed shoreline. Sunlight exposure and reduced anthropogenic disturbance evidently promoted a broader range of species. In contrast, fewer species were found in transects T2 and T6, likely influenced by process water input (T2) or shading from riparian vegetation (T6). Everywhere, macrophyte abundance peaked at 1–2 m water depth and was lower at 0–1 m, possibly due to light oversaturation (Schwoerbel and Brendelberger, 2013) or sediment deposition on unstable slopes, which both may hinder growth. Below 2 metres, macrophyte abundance declined sharply. The distribution was limited to the littoral zone, with an average depth of 5.25 m (±0.52 m). No macrophyte growth was observed beneath the FPV system. The low abundance of habitat-typical species indicates an ecologically compromised lake condition, which is typical for anthropogenic gravel pit lakes. In these lakes, several factors (*e.g.,* steep shorelines, shoreline erosion, increased sedimentation from process water) likely constrain macrophyte expansion, independent of FPV (Mollema and Antonelli, 2016). Furthermore, high cyprinid densities may contribute to sediment resuspension and herbivory, suppressing macrophyte growth (Hansson *et al.*, 1987; Zambrano and Hinojosa, 1999; Yuan, 2021). In all lakes, the trophic state plays a major role for macrophytes. Oligotrophic systems generally support a more extensive LML, while eutrophication reduces light penetration and restricts submerged vegetation. In Lake Leimersheim, the installed FPV system affected local light conditions, but the primary constraints on macrophyte distribution were driven by other factors such as lake morphology, sediment loading, and fish community composition. These existing conditions supposedly overrode potential FPV-related effects, highlighting the need for a comprehensive assessment of site-specific ecological constraints before attributing changes in macrophyte dynamics to FPV.

4.4 Hydrodynamic modelling and FPV impact analysis

4.4.1 Model performance and applicability

Both GLM-AED2 and Delft3D-FLOW effectively simulated the hydrodynamics of our gravel pit lake. On the one hand, Delft3D-FLOW provided detailed local FPV impact

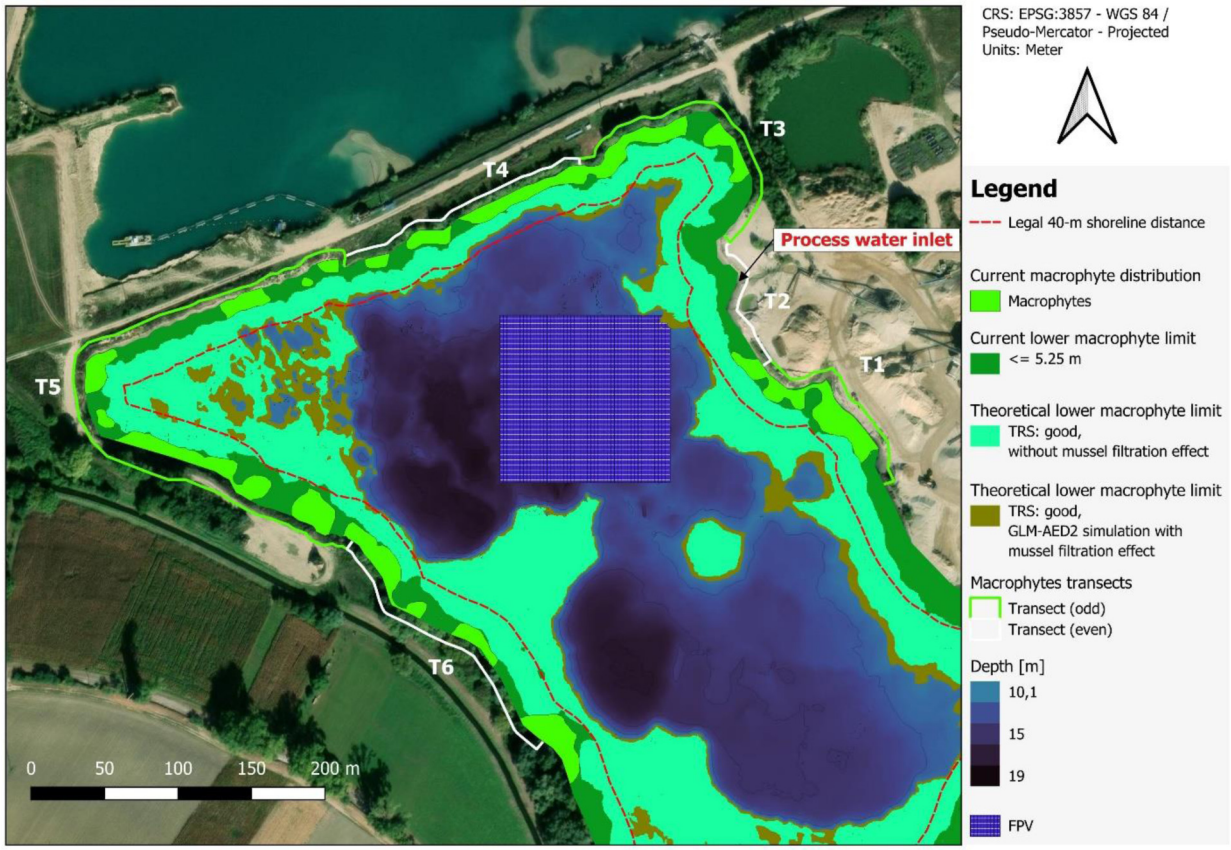

Fig. 13. Current macrophyte distribution (light green areas) and lower macrophyte limit (dark green areas). The potential macrophyte distribution (turquoise area) corresponds to the theoretical lower macrophyte limit under good ecological conditions (Trophic Reference State) as defined by the European Water Framework Directive. Mussel filtration by colonies attached to the 58 % FPV system—covering the macrophyte-free zone as simulated by GLM-AED2—resulted in an expanded macrophyte distribution (brown area). The legal 40 m shoreline distance is marked with a red dashed line.

predictions but required significantly more computational time, limiting scenario-based ecological analyses. Its simulated flow velocity remained uncertain and would require validation, such as with upward-looking Acoustic Doppler Current Profiler measurements (Parsapour-Moghaddam and Rennie, 2017; Goulart *et al.*, 2023). Nevertheless, Delft3D-FLOW appears to be a good choice for heterogeneous lakes or small FPV systems in large water bodies. On the other hand, GLM-AED2, while assuming horizontal homogeneity, proved effective for advanced FPV impact assessments, offering high computational efficiency (Ishikawa *et al.*, 2022; Amorim et al., 2023). GLM-AED2 can approximate species distribution using a quasi-2D approach, making it useful for multi-lake assessments, climate change simulations, and FPV design evaluation. The choice between models depends on the required level of detail: Delft3D-FLOW is preferable for local assessments in complex lakes, while GLM-AED2 is more efficient for large-scale FPV scenarios. Combining the two models may provide synergistic benefits, leveraging their respective strengths. Optimising hydrodynamic models for FPV is still in its early stages but will depend on detailed monitoring data sets.

4.4.2 Thermal and ecological impacts of FPV coverage scenarios

empirical and modelling studies consistently show that FPV installations reduce lake surface water temperature, though the extent varies with lake characteristics, FPV coverage, and methodology. Nobre *et al.* (2025) measured a 1.2 °C annual mean reduction, peaking at 3.0 °C on the warmest days in French gravel pit lakes, while Ilgen *et al.* (2023) recorded a 2.8 °C cooling in a German gravel pit lake during summer. Modelling studies predicted a broader range. Exley *et al.* (2021) simulated 8.0 °C cooling in Windermere, UK, and Ji *et al.* (2022) estimating a 3.3 °C reduction in the Xiangjiaba Reservoir, China. The present results fell within this range, as GLM-AED2 predicted a 3.6 °C reduction and Delft3D-FLOW a stronger 7.2 °C reduction at 90% FPV coverage. FPV-induced cooling also affects lake stratification, weakening Schmidt stability and altering mixing regimes. Ilgen *et al.* (2023) found little impact below 15% FPV, with significant shifts beyond 50% coverage, a threshold also supported by the present study. Both simulation models indicated a decline in Schmidt stability for high FPV

occupancies, which was accompanied by a thermocline shift to shallower depths. The TSI in GLM-AED2 declined with increasing FPV coverage, though considerable changes only occurred beyond 45% FPV. Yang *et al.* (2022) reported reduced chlorophyll-*a* and primary production in a tropical reservoir at 30% FPV coverage, while Karpouzoglou *et al.* (2020) found significant declines already above 20%. These numbers suggest that FPV effects on lake ecology depend on the individual lake but may counteract global warming-induced stratification intensification (Woolway *et al.*, 2020), which enhances nutrient retention in the epilimnion and primary production (O'Beirne *et al.*, 2017).

4.4.3 Implications of mussel filtration for macrophyte dynamics in FPV-integrated lake restoration

Given a 25–30-year service life, FPV systems may outlast anthropogenic influences like gravel extraction, highlighting the need to integrate lake renaturation into FPV planning. We used GLM-AED2 to simulate macrophyte distribution, applying a quasi-2D approach calibrated to the WFD trophic reference state. We also incorporated mussel filtration effects at the FPV structure, showing its potential to influence lake-wide ecological dynamics. Mussels primarily colonise FPV substructures, but their filtration extends across the entire lake, improving water clarity and promoting macrophyte expansion, counteracting eutrophication.

Ray *et al.* (2024) demonstrated that improper FPV placement, particularly over macrophyte-dominated areas, can also result in negative effects, such as reduced oxygen levels and increased greenhouse gas emissions, likely due to the decomposition of macrophytes. This highlights the importance of optimised FPV siting and calls for adequate simulation of potential impacts before new systems are installed.

4.5 Regulatory considerations for FPV placement

In Germany, FPV installations are subject to a regulatory limit of 15% lake surface coverage and a minimum shoreline distance of 40 metres. For the FPV system at Lake Leimersheim, the observed distance to LML was approximately 35 metres, while the theoretical LML, derived from the trophic reference state, extended up to 200 metres. This discrepancy suggests that fixed-distance regulations may not consistently reflect the depth-dependent distribution of macrophytes, particularly in artificial lakes with steep bathymetry and heterogeneous morphometry. In addition, active sediment input and anthropogenic shoreline modification can influence aquatic vegetation independently of FPV siting. These factors may also vary over time, depending on the lake's stage of ecological succession.

Model simulations using Delft3D-FLOW and GLM–AED2 indicated that substantial alterations in lake stratification and water quality only occurred at FPV coverages above 45%. This modelled response differs markedly from the regulatory threshold, suggesting that fixed limits may not uniformly correspond to ecological effects across different lake types. The interpretation of such thresholds thus appears to depend on local morphometric and ecological characteristics, as well as on the specific FPV design and coverage.

5 Conclusions

This study assessed an FPV system covering 8% of a gravel pit lake in southwest Germany and found no major ecological impacts. External stressors, such as sediment-rich inflows and herbivorous fish, exerted a stronger influence on water quality and macrophyte growth than the FPV installation itself. Colonisation of the FPV substructure by invasive mussels improved water clarity and promoted macrophyte growth, indicating possible synergies with lake restoration. However, ecological risks remain and require site-specific evaluation. Hydrodynamic model simulations (Delft3D-FLOW and GLM-AED2) showed substantial changes in lake dynamics only above 45% FPV coverage. These findings suggest that the current regulatory framework in Germany – limiting FPV installations to 15% surface coverage and a 40-metre shoreline buffer – though precautionary, may be overly conservative for artificial lakes subject to strong external pressures. This study calls for more flexible, site-specific regulations that account for lake depth, morphometry, and trophic state. Classification-based thresholds should reflect lake type, usage, and ecological status. Expert assessments combining empirical field data and modelling may offer ecologically sound alternatives to fixed criteria. Such flexibility would enable context-sensitive FPV integration. Further empirical and modelling studies are needed to support this approach.

Acknowledgements

The authors kindly thank Erdgas Südwest GmbH, which offered the FPV system for research purposes. In addition, our thanks go to the Pfadt GmbH Kieswerk-Baustoffe, which provided unrestricted and safe access to the study site. We also thank Annie Schlöffel for her support in the field and laboratory during the sampling and monitoring of the biofilm and mussels. Finally, the authors acknowledge the support of the technical team at Fraunhofer ISE during the installation and maintenance of the monitoring system.

Funding

K.I. was supported by a scholarship from the German Federal Foundation for the Environment (DBU, no. 08020211210/002). The researchers of Fraunhofer ISE acknowledge the support from the FPV4Resilience project, funded by the Sustainability Center Freiburg (LZN). This study was financed in part by the Coordenação de Aperfeiçoamento de Pessoal de Nível Superior – Brasil (CAPES) – Finance Code 001. C.G. was supported by a sandwich doctorate scholarship by the Coordination for the Improvement of Higher Education Personnel (CAPES) during her time in Germany – CAPES-PrInt, call no. 01/2022 CAPES-PRINT-UFPR – Sandwich Doctorate. T. B. acknowledges the productivity stipend from the National Council for Scientific and Technological Development – CNPq, grant no. 313491/2023-2, call no. 09/2023.

Competing interest

The authors have no relevant financial or non-financial interests to disclose.

References

Amorim LF, Duarte BPDS, Martins JRS. 2023. Comparison between methods to predict climate change impacts on tropical shallow lakes. *J Water Clim Change* 14: 4299–4313.

Benjamins S, Williamson B, Billing S-L, Yuan Z, Collu M, Fox C, Hobbs L, Masden EA, Cottier-Cook EJ, Wilson B. 2024. Potential environmental impacts of floating solar photovoltaic systems. *Renew Sustain Energy Rev* 199: 114463.

Bundesamt für Justiz. 2023. §36 WHG – Einzelnorm. Available from: https://www.gesetze-im-internet.de/whg_2009/__36.html (last consult: 2024/10/10).Carlson RE. 1977. A trophic state index for lakes. *Limnol Oceanogr* 22: 361–369.

Château P-A, Wunderlich RF, Wang T-W, Lai H-T, Chen C-C, Chang F-J. 2019. Mathematical modeling suggests high potential for the deployment of floating photovoltaic on fish ponds. *Science of The Total Environment* 687: 654–666.

Connelly NA, O'Neill CR, Knuth BA, Brown TL. 2007. Economic impacts of zebra mussels on drinking water treatment and electric power generation facilities. *Environmental Management* 40: 105–112.

Dalderup T, Van Leijsen M, Meppelink M, Van den Oord T, Richardson T, Verdonk M, Van Zeil V. 2020. Aquaculture activities in energy storage lake: advice for cultivating shellfish and seaweed in combination with a floating solar park. *Aquaculture in Delta21 Energy Storage Lake Final Report*. Available from: https://www.delta21.nl/wp-content/uploads/2020/06/AQUACULTUUR-rapport.pdf

de Lima RLP, Paxinou K, C. Boogaard F, Akkerman O, Lin FY. 2021. In-situ water quality observations under a large-scale floating solar farm using sensors and underwater drones. *Sustainability* 13: 6421.

Deltares. 2024. Delft3D-FLOW: transport phenomena, including sediments – User manual hydro-morphodynamics.

Diggins T.P. 2001. A seasonal comparison of suspended sediment filtration by quagga (*Dreissena bugensis*) and zebra (*D. polymorpha*) mussels. *J Great Lakes Res* 27: 457–466.

Exley, G., Armstrong, A., Page, T., Jones, I.D. 2021. Floating photovoltaics could mitigate climate change impacts on water body temperature and stratification. *Solar Energy* 219:, 24–33.

Exley G, Page T, Thackeray SJ, Folkard AM, Couture R-M, Hernandez RR, Cagle AE, Salk KR, Clous L, Whittaker P, Chipps M, Armstrong, A. 2022. Floating solar panels on reservoirs impact phytoplankton populations: A modelling experiment. *Journal of Environmental Management* 324, 116410.

Goulart, C.B., Bleninger, T., de Oliveira Fagundes, H., Fan, F.M. 2023. Modeling uncertainties of reservoir flushing simulations. *International Journal of Sediment Research* 38, 698–710.

Gren, I.-M., Lindahl, O., Lindqvist, M. 2009. Values of mussel farming for combating eutrophication: An application to the Baltic Sea. *Ecological Engineering* 35, 935–945.

Haag, W.R., Williams, J.D., 2014. Biodiversity on the brink: an assessment of conservation strategies for North American freshwater mussels. *Hydrobiologia* 735, 45–60.

Haas, J., Khalighi, J., De La Fuente, A., Gerbersdorf, S.U., Nowak, W., Chen, P.-J. 2020. Floating photovoltaic plants: Ecological impacts versus hydropower operation flexibility. *Energy Conversion* and Management 206: 112414.

Hansson L.-A., Johansson L., Persson L. 1987. Effects of fish grazing on nutrient release and succession of primary producers. *Limnol Oceanogr* 32: 723–729.

Hipsey M.R. 2022. Modelling aquatic eco-dynamics: Overview of the AED modular simulation platform. Available from: https://doi.org/10.5281/ZENODO6516222

Hipsey M.R., Bruce L.C., Boon C., Busch B., Carey C.C., Hamilton D.P., Hanson P.C., Read J.S., de Sousa E., Weber M., Winslow L.A. 2019. A general lake model (GLM 3.0) for linking with high-frequency sensor data from the Global Lake Ecological Observatory Network (GLEON). *Geosci. Model Dev.* 12: 473–523.

Idso S.B. 1973. On the concept of lake stability. *Limnol. Oceanogr.* 18: 681–683.

Ilgen, K., Schindler, D., Wieland, S., Lange, J., 2023. The impact of floating photovoltaic power plants on lake water temperature and stratification. *Sci Rep* 13:, 7932.

Ishikawa M., Gonzalez W., Golyjeswski O., Sales G., Rigotti J.A., Bleninger T., Mannich M., Lorke A. 2022. Effects of dimensionality on the performance of hydrodynamic models for stratified lakes and reservoirs. *Geosci. Model Dev.* 15: 2197–2220.

Ji Q., Li K., Wang Y., Feng J., Li R., Liang R. 2022. Effect of floating photovoltaic system on water temperature of deep reservoir and assessment of its potential benefits: a case on Xiangjiaba Reservoir with hydropower station. *Renewable Energy* 195: 946–956.

Kakoulaki G., Gonzalez Sanchez R.Gracia Amillo A. Szabo S. De Felice M. Farinosi F. De Felicek L. Bisselin B. Seliger R. Kougias I. Jaeger-Waldau A. 2023. Benefits of pairing floating solar photovoltaics with hydropower reservoirs in Europe. *Renewable and Sustainable Energy Reviews* 171: 112989.

Karpouzoglou T., Vlaswinkel B., van der Molen J. 2020. Effects of large-scale floating (solar photovoltaic) platforms on hydrodynamics and primary production in a coastal sea from a water column model. *Ocean Science* 16: 195–208.

Ladwig R, Hanson PC, Dugan HA, Carey CC, Zhang Y, Shu L, Duffy CJ, Cobourn KM. 2021. Lake thermal structure drives interannual variability in summer anoxia dynamics in a eutrophic lake over 37 years. *Hydrol Earth Syst Sci* 25: 1009–1032.

Lee N, Grunwald U, Rosenlieb E, Mirletz H, Aznar A, Spencer R, Cox S. 2020. Hybrid floating solar photovoltaics-hydropower systems: Benefits and global assessment of technical potential. *Renewable Energy* 162: 1415–1427.

Lei J, Payne BS, Wang SY. 1996. Filtration dynamics of the zebra mussel, Dreissena polymorpha. *Can. J. Fish. Aquat. Sci.* 53: 29–37.

Li W, Wang Y, Wang G, Liang Y, Li C, Svenning JC. 2023. How do rotifer communities respond to floating photovoltaic systems in the subsidence wetlands created by underground coal mining in China? *J. Environ. Manag.* 339: 117816.

Liu X, Zhang Y, Shi K, Lin J, Zhou Y, Qin B. 2016. Determining critical light and hydrologic conditions for macrophyte presence in a large shallow lake: The ratio of euphotic depth to water depth. *Ecol. Indic.* 71: 317–326.

Matthews J, Van der Velde G, Bij de Vaate A, Collas FPL, Koopman KR, Leuven RSEW. 2014. Rapid range expansion of the invasive quagga mussel in relation to zebra mussel presence in The Netherlands and Western Europe. *Biol. Invasions* 16: 23–42.

Mollema, Pauline N., and Marco Antonellini. 2016. Water and (bio) chemical cycling in gravel pit lakes: A review and outlook. *Earth-Science Reviews* 159: 247–270

NASA. 2023. POWER | Data Access Viewer [WWW Document]. Available from: https://power.larc.nasa.gov/data-access-viewer/ (accessed 3 August 2023).

Nobre R, Boulêtreau S, Colas F, Azemar F, Tudesque L, Parthuisot N, Favriou P, Cucherousset J. 2023. Potential ecological impacts of floating photovoltaics on lake biodiversity and ecosystem functioning. *Renewable and Sustainable Energy Reviews* 188: 113852.

Nobre R, Rocha SM, Healing S, Ji Q, Boulêtreau S, Armstrong A, Cucherousset J. 2024. A global study of freshwater coverage by floating photovoltaics. *Solar Energy* 267: 112244.

Nobre RLG, Vagnon C, Boulêtreau S, Colas F, Azémar F, Tudesque L, Parthuisot N, Millet P, Cucherousset J. 2025. Floating photovoltaics strongly reduce water temperature: A whole-lake experiment. *Journal of Environmental Management* 375: 124230.

O'Beirne MD, Werne JP, Hecky RE, Johnson TC, Katsev S, Reavie ED, 2017. Anthropogenic climate change has altered primary productivity in Lake Superior. *Nature communications* 8: 15713.

Ogunjo S, Olusola A, Olusegun C. 2023. Potential of using floating solar photovoltaic and wind farms for sustainable energy generation in an existing hydropower station in Nigeria. *Clean Techn Environ Policy* 25: 1921–1934.

Orlova MI, Muirhead JR, Antonov PI, Shcherbina GK, Starobogatov YI, Biochino GI, Therriault TW, MacIsaac HJ. 2004. Range expansion of quagga mussels *Dreissena rostriformis bugensis* in the Volga River and Caspian Sea basin. *Aquatic Ecology* 38: 561–573.

Parsapour-Moghaddam P, Rennie Cd. 2017. Hydrostatic versus nonhydrostatic hydrodynamic modelling of secondary flow in a tortuously meandering river: Application of Delft3D. *River Research and Applications* 33: 1400–1410.

Petersen JK, Hasler B, Timmermann K, Nielsen P, Tørring DB, Larsen MM, Holmer M. 2014. Mussels as a tool for mitigation of nutrients in the marine environment. *Marine Pollution Bulletin* 82: 137–143.

Ray NE, Holgerson MA, Grodsky SM. 2024. Immediate effect of floating solar energy deployment on greenhouse gas dynamics in ponds. *Environmental Science & Technology* 58: 22104–22113.

Roditi HA, Caraco NF, Cole JJ, Strayer DL. 1996. Filtration of Hudson River water by the zebra mussel (Dreissena polymorpha). *Estuaries* 19: 824.

Rowe MD, Anderson EJ, Vanderploeg HA, Pothoven SA, Elgin AK, Wang J, Yousef F. 2017. Influence of invasive quagga mussels, phosphorus loads, and climate on spatial and temporal patterns of productivity in Lake Michigan: A biophysical modeling study. *Limnology and Oceanography* 62: 2629–2649.

Schmidt W. 1928. Über die Temperatur und Stabilitätsverhältnisse von Seen. *Geografiska Annaler* 10: 145–177.

Schwoerbel J, Brendelberger H. 2013. *Einführung in die Limnologie*, 10th ed.Berlin Heidelberg: Springer Spektrum.

Son M. 2007. Native range of the zebra mussel and quagga mussel and new data on their invasions within the Ponto-Caspian Region. *AI* 2:, 174–184.

Soto D, Mena G. 1999. Filter feeding by the freshwater mussel, *Diplodon chilensis*, as a biocontrol of salmon farming eutrophication. *Aquaculture* 171: 65–81.

van de Weyer K, Stelzer D. 2021. Handlungsanweisung zur WRRL-Bewertung von Makrophyten in Seen nach dem NRW-Verfahren. Available from: https://www.laenderfinanzierungsprogramm.de/static/LFP/Dateien/LAWA/AO/O_2.20_Handlungsanweisung%20NRW%20Verfahren%20Makrophyten%20Seen%20WRRL%20Stand%20Oktober%202021.pdf.

Varelas K, Auger A, Brockhoff D, Hansen N, ElHara OA, Semet Y, Kassab R, Barbaresco F. 2018. A comparative study of large-scale variants of CMA-ES, in: *Parallel Problem Solving from Nature-PPSN XV: 15th International Conference, Coimbra, Portugal*, September 8-12, 2018, Proceedings, Part I 15. Springer, pp. 3–15. Available from: https://doi.org/10.1007/978-3-319-99253-2_1.

Ward, G.J. 1994. The RADIANCE lighting simulation and rendering system. In: *Proceedings of the 21st Annual Conference on Computer Graphics and Interactive Techniques – SIGGRAPH '94. Presented at the 21st annual conference*, ACM Press, Not Known, pp. 459–472.

Wegner, B., Kronsbein, A.L., Gillefalk, M., van de Weyer, K., Köhler, J., Funke, E., Monaghan, M.T., Hilt, S. 2019. Mutual facilitation among invading Nuttall's waterweed and quagga mussels. *Front. Plant Sci*. 10. Available from: https://doi.org/10.3389/fpls.2019.00789.

Winslow, L., Albers, S., DougCollinge, Read, J.S., Leach, T., Zwart, J., Snortheim. 2018. Gleon/Rlakeanalyzer: Rlakeanalyzer 1.11.4. Available from: https://doi.org/10.5281/ZENODO.1198428.

Wirth, H., Eggers, J.-B., Trommsdorf, M., Neuhaus, H., Heinrich, M., Wieland, S., Schill, C. 2021. Potenziale der Integrierten Photovoltaik in Deutschland. Fraunhofer ISE, Freiburg. Available from: https://www.ise.fraunhofer.de/de/geschaeftsfelder/solarkraftwerke-und-integrierte-photovoltaik/integrierte-photovoltaik.html.

Woolway RI, Kraemer BM, Lenters JD, Merchant CJ, O'Reilly CM, Sharma S. 2020. Global lake responses to climate change. *Nature Reviews Earth & Environment* 1: 388–403.

World Bank Group, ESMAP, SERIS. 2019a. Where Sun Meets Water: Floating Solar Handbook for Practitioners. WorldBank, Washington DC. Available from: http://documents.worldbank.org/curated/en/418961572293438109/Where-Sun-Meets-Water-Floating-Solar-Handbook-for-Practitioners

World Bank Group, Energy Sector Management Assistance Program, Solar Energy Research Institute of Singapore. 2019b. Where sun meets water – floating solar market report. © World Bank, Washington, DC. Available from: http://documents.worldbank.org/curated/en/579941540407455831/Floating-Solar-Market-Report-Executive-Summary

Xia Z, Li Y, Guo S, Chen R, Zhang W, Zhang P, Du P. 2023. Mapping global water-surface photovoltaics with satellite images. *Renewable and Sustainable Energy Reviews* 187: 113760.

Yang P, Chua LHC, Irvine KN, Nguyen MT, Low EW. 2022. Impacts of a floating photovoltaic system on temperature and water quality in a shallow tropical reservoir. *Limnology* 23: 441–454.

Yu N, Culver DA. 2001. Estimating the effective clearance rate and refiltration by zebra mussels, Dreissena polymorpha, in a stratified reservoir. *Freshwater Biology* 41: 481–492.

Yuan LL. 2021. Continental-scale effects of phytoplankton and non-phytoplankton turbidity on macrophyte occurrence in shallow lakes. *Aquatic sciences* 83: 14.

Zambrano L, Hinojosa D. 1999. Direct and indirect effects of carp (*Cyprinus carpio* L.) on macrophyte and benthic communities in experimental shallow ponds in central Mexico. *Hydrobiologia* 408: 131–138.

Cite this article as: Ilgen K, Goulart CB, Hilgert S, Schindler D, van de Weyer K, de Carvalho Bueno R, Bleninger T, Lastrico R, Gfüllner L, Graef A, Fuchs S, Lange J. 2025. Hydrological and ecological effects of floating photovoltaic systems: a model comparison considering mussel, periphyton, and macrophyte growth. *Knowl. Manag. Aquat. Ecosyst.*, 426, 11. https://doi.org/10.1051/kmae/2025008